8th U. S. National Combustion Meeting
Organized by the Western States Section of the Combustion Institute
and hosted by the University of Utah
May 19-22, 2013

Effect of Varying the Initial Diameter of n-Octane and n-Decane Droplets over a Wide Range on the Spherically Symmetric Combustion Process: International Space Station and Ground-based Experiments

Yu Cheng Liu[1], *Koffi N. Trenou*[1], *Jeff Rah*[1], *Michael C. Hicks*[2], *C. Thomas Avedisian*[1]

[1]*Sibley School of Mechanical and Aerospace Engineering, Cornell University, Ithaca, NY 14853.*
[2]*NASA Glenn Research Center, Cleveland, OH 44135.*

This study reports on an investigation of varying the initial droplet diameter (D_o) over a very wide range (from 0.5 mm to 5 mm) on droplet combustion. The droplet burning history is examined in an environment of reduced convection as promoted by low gravity to achieve spherical droplet flames. The fuels examined are n-octane and n-decane. The long burning times for $D_o > 1.2$ mm were accommodated in the Multi-user Droplet Combustion Apparatus (MDCA) onboard the orbiting International Space Station (ISS), while experiments for $D_o < 1$ mm were carried out in a ground-based drop tower. The results reported encompass the widest range of D_o examined in the history of droplet combustion experimentation for a given fuel. Both free floating (unsupported) and fiber-supported droplets are deployed and ignited. Quantitative data are obtained from digital analysis of the individual video images of the burning process for the droplet, flame and soot shell diameters.

Results show that the droplet burning rate decreases with increasing D_o throughout the D_o range investigated. The mechanisms responsible include a combination of fuel molecule residence time effects and radiative losses from the flame, both of which influence soot formation to varying degrees. Assuming that increasing soot formation (e.g., from increasing residence times) would lower heat transfer to the droplet, "small" droplets ($D_o < 1$ mm, with negligible radiation losses) will burn slower as D_o increases in this initial droplet diameter range, which is consistent with the experimental results. For $D_o > 1.5$ mm the droplet flames appeared less luminous and therefore less sooty, yet the droplets continued to burn progressively slower as D_o increased. This effect is conjectured to be the result of increased radiative losses that would tend to reduce sooting that outweigh the longer residence times of the larger droplets that would tend to increase sooting. The experimental results reported also include the evolution of relative distances between the flame, soot shell, and droplet diameters, all of which are influenced by D_o.

1. Introduction

Droplet combustion has been extensively studied since the early work of Godsave (1953). This long-standing interest stems from the need to better understand combustion of fuel sprays using a simpler combustion configuration that, at the same time, includes effects found in sprays such as complex combustion chemistry, fuel evaporation processes, phase equilibrium behavior, moving boundaries, and transient effects. The base case of spherical symmetry is ideal for this purpose. Figure 1 shows the droplet flame structure for this configuration. It consists of the droplet, a soot shell that may form (depending on the fuel type) and the flame all of which would be spherical and concentric for this ideal case.

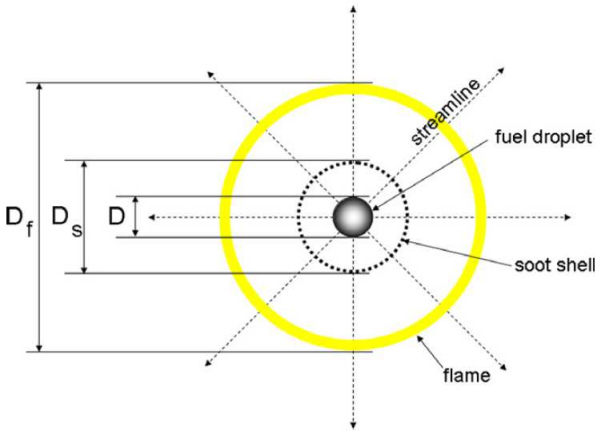

Figure 1. Schematic of a spherically symmetric droplet flame structure.

The classical droplet combustion theory (Turns (1999)) for the case of no soot formation or radiative effects, and quasi-steadiness in the gas and liquid transport process, leads to the well-known prediction that $(D/D_o)^2 = 1\text{-}K_o t/D_o^2$ where D is the droplet diameter, t is time, and K_o represents the burning rate value. As suggested, the square of droplet diameter should decrease linearly with time with K_o being constant (hence the rationale for scaling the droplet diameter as $(D/D_o)^2$ and the time as t/D_o^2 in the presentation of the quantitative measurements discussed in Section 3). The reality of droplet burning as shown by many studies for the based of Fig. 1 (e.g., Jackson et al. (1992, 1994); Avedisian (2000); Lee et al. (1998); Bae and Avedisian (2009)) is different.

The influence of initial droplet diameter on K_o, in particular, has been stimulated by its potential importance on the droplet burning process. Figure 2a is a schematic of some of the trends reported. Early studies (Kumagai et al. (1971); Hara and Kumagai (1994)) first employed unsupported or freely-floating droplets to study the effect of D_o on the droplet burning rate. The results showed a slight increase of K_o with D_o. Later work (Jackson et al. (1992, 1994); Lee et al. (1998) suggested that K_o decreases with increasing D_o.

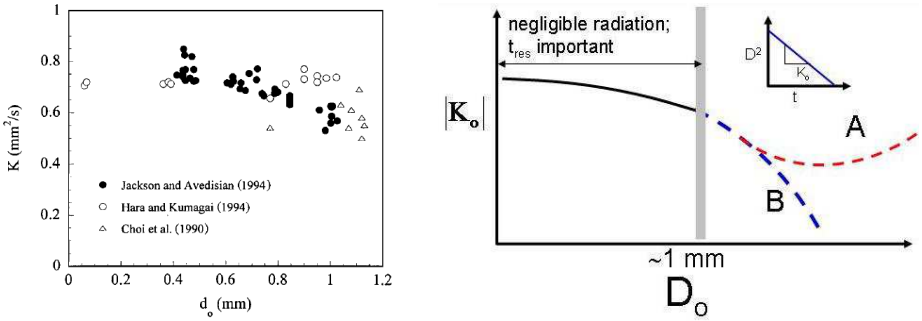

Figure 2. (a) Experimental data (Lee et al. 1998) showing the dependency of burning rate K on the initial droplet diameter D_o for smaller droplet diameters (D_o < 1.2 mm); (b) Speculations for dependency of burning rate K in the larger droplet diameter range: A: K increases due to less soot formation, B: K decreases due to more soot formation.

The mechanisms responsible for an influence of D_o on K_o are speculative. They appear to principally include a combination of fuel molecule residence time between the droplet surface and flame, and radiative loss effects that would be expected to conceptually influence soot formation and heat transfer to the droplet. For D_o < 1 mm radiation should be negligible (Marchese et al. (1998)) and soot formation alone may be responsible for an influence of D_o on K_o. Radiative losses become more significant for D_o > 1 mm, while the residence time continues to increase with D_o suggesting that either of the trends in Fig. 2b ("A" or "B") could be viable. To date, no data have been reported for D_o > 1 mm with complete burns to elucidate the transition in potential mechanisms controlling K_o.

To provide a more complete picture of the influence of D_o on burning, ground-based experiments were carried in conjunction with ISS experiments (Fig. 3a) to investigate the combined range 0.5 mm < D_o < 5.0 mm. The fuels are n-octane and n-decane, as they are relevant components in gasoline and jet fuel surrogates, and have favorable attributes associated with the ability to predict their thermal properties as well as combustion chemistries that are known. Figures 3b and 3c depict selected photographs of the droplet, flame and soot shell structure typical of free-floating droplets from the ISS experimental platform. A typical spherically symmetric droplet flame for sooty fuels (Fig. 3b) consists of an

inner yellow (or brighter color depending on the lens and camera settings) flame indicating soot incandescence and an outer blue zone. The broad characteristics shown are consistent with the idealization of Fig. 1.

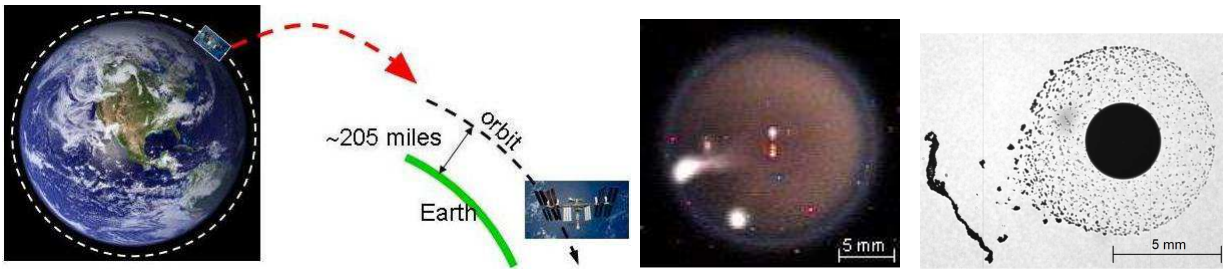

Figure 3. (a) Illustration of the International Space Station (ISS) orbiting around the Earth; (b) a spherically symmetric n-decane droplet flame from the microgravity experiments on the ISS (D_o = 3.03 mm); (c) a black-and-white picture of a burning n-decane droplet (D_o = 3.95 mm) showing the breakage of the soot tail and the intact symmetry of the soot shell.

2. Experimental Methods

In order to achieve nearly spherical droplet flames, the experiments are carried out in a low gravity environment with experimental designs that restrict droplet motion. For 0.52 mm < D_o < 0.85 mm, a ground-based 1.2 s drop tower was used, while for D_o > 1.7 mm the Multi-user Droplet Combustion Apparatus (MDCA) onboard the orbiting ISS provided the long time conditions needed to observe the complete burning process. In the range 0.85 mm < D_o < 1.7 mm no data are reported because GB experiments were limited to 1.2 s of experimental time and ISS experiments were difficult to carry out for droplets close to about D_o = 1.5 mm because of issues with droplet deployment that could impart a significant velocity to the droplets to move them out of the imaging field of view. The experimental conditions were room temperature air at atmospheric pressure. A brief description of each facility is given in the following discussion.

2.1 Ground-based (GB) Experiments

Briefly, a test droplet is created by a droplet generator and anchored on the cross of two SiC (14 μm) fiber filaments in a sealed combustion chamber filled with atmospheric pressure air. The size of the test droplet is controlled by merging several fuel droplets until the desired D_o is achieved. The supported droplet is then subjected to a low gravity environment by releasing the entire instrumentation package (the inner package with imaging systems, power supplies, and spark circuitry, and the outer serving as a "drag shield") into free fall. To reduce the disturbance attributed to package release, 300 ms after free fall begins the test droplet is ignited by two symmetric sparks generated by two pairs of spark electrodes on the sides of the droplet. The spark electrodes are retracted immediately after sparks are fired in order not to influence the flame. Modeling of the droplet burning process on the small fibers employed for D_o of about 0.5 mm (Liu et al. (2013)) showed a minimal effect on the burning process.

The timing of the processes is pre-programmed and triggered using a multi-channel signal generator (QC-9618, Quantum Composer). The burning process of fuel droplets is recorded simultaneously by a black-and-white (BW) high speed camera (MS-80K, CPL Inc., 200 fps, 3.9 MP) and a color camera (Hitachi HV-C20, 30 fps, 0.3 MP) from different angles. Figure 4a shows the layout of the instrumentation package, and Fig. 4b illustrates the experimental procedures associated with drop tower experiments. More details can be found in Liu and Avedisian (2012).

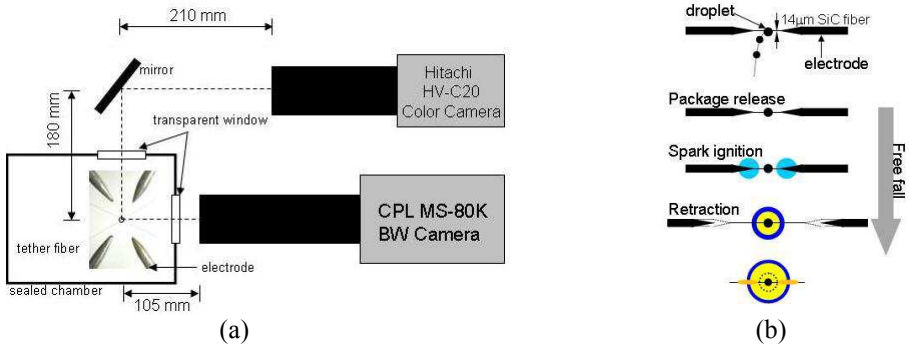

Figure 4. (a) Layout of the inner instrumentation package for drop tower experiments. (b) Experimental procedures for a drop tower experiment.

2.2 ISS Experiments

The MDCA onboard the orbiting ISS is a facility that allows burning fuel droplets to be studied in various ambiences with or without a supporting fiber (currently 80 μm diameter). Figure 5 shows a series of schematics of the experimental apparatus and the procedure for forming and deploying free-floating droplets on the MDCA.

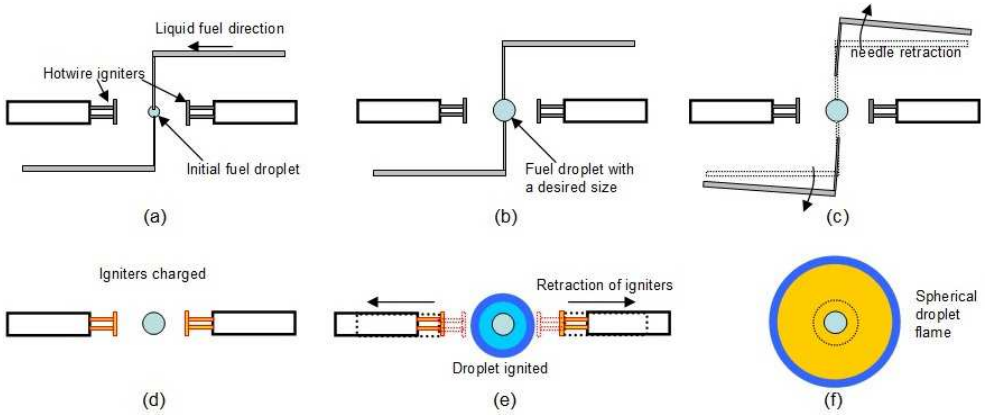

Figure 5. Experimental procedures for the droplet combustion experiments on the International Space Station (ISS) (a) droplet formation; (b) initial diameter control; (c) needle retraction; (d) hotwire charging; (e) igniter retraction; (f) droplet burning with spherical symmetry.

Fuel is deployed through hollow needles which are then stretched slightly to form a liquid bridge that essentially pre-stresses the droplet until the desired droplet size is reached (Figs. 5a and 5b). The needles are then quickly retracted leaving the (ideally) stationary liquid droplet behind (Fig. 5c). In reality there is some small drift associated with uneven motion of the needles. In the present study, only deployments in which the droplet stayed within the camera field of view are reported. Hotwire igniters are then energized (Fig. 5d) and retracted when the droplet is ignited (Fig. 5e). The droplet flame in the MDCA is recorded by a Hi-Beam camera (1 MP at 30 fps) with an infrared laser diode as a backlight and a color camera (0.3 MP at 30 fps). A low light level ultra violet (LLLUV) camera provides OH emission boundaries.

All the images are temporarily stored on the "image processing and storage units" (IPSUs) and downloaded to a ground-based computer. The MDCA also has capability to deploy an 80 μm tether fiber (SiC) to examine the influence on the support fiber. The time sequence of the above described procedures is pre-programmed for each test and remotely controlled by the NASA Glenn Research Center in Cleveland, OH. The live video of each experiment is fed to PCs in NASA Glenn and Cornell to instantaneously monitor the experiments in real time.

2.3 Image analysis

The main diagnostic of the experiments reported here are the digital video cameras that record the droplet burning history. The images obtained from the ground-based experiments and ISS experiments are processed in a similar fashion. Figure 6 shows how the dimensions of interest are extracted from the digital images for droplet, soot shell, and flame diameters.

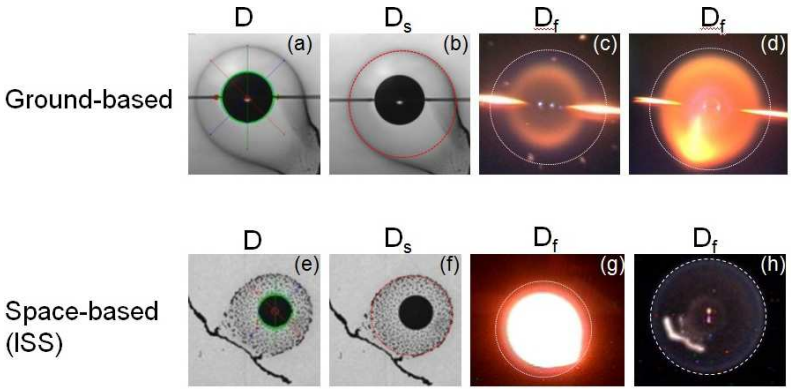

Figure 6. Dimension extraction process for obtaining droplet diameter D, soot shell diameter D_s and flame diameters D_f for ground-based experiments (from a to d) and ISS experiments (from e to h).

For the ground-based experiments, the droplet diameters (Fig. 6a) are extracted from the BW high speed camera images using a Matlab program (Dembia et al. (2012)). The green circle in Fig. 6a outlines the measurement generated by the program. Figure 6b shows the manual measurement for a soot shell diameter. Because n-octane and n-decane both produce a considerable amount of soot aggregates during burning, the process of local soot accumulation sometimes randomly breaks the symmetry of an intact soot shell. While this phenomenon does not affect the flame symmetry, the asymmetric part of a soot shell is ignored in the soot shell diameter measurements, as shown by the bottom right corner of the red dotted circle in Fig. 6b. BW images from the Hi-Beam camera of the MDCA are used to obtain droplet diameters and soot shell diameters using similar methods described above for ground-based images (see Figs. 6e and 6f).

For the ground-base flame images, the outer edge of the blue flame (Fig. 6c) is used as the "flame" diameter. This defined flame diameter is not affected by the distortion of the inner yellow flame (due to asymmetry of soot aggregation, see Fig. 6d). For the ISS flames, a different lens setting provides flame images that are over-saturated near the ignition point. A definite boundary outside of the inner bright core (Fig. 6g) can still be identified for flame diameters. Nonetheless, a typical n-octane or n-decane droplet flame has a blue boundary that can be easily measured as shown in Fig. 6h.

3. Results and Discussion

Figure 7 shows selected flame images for n-octane droplets from both the ISS and GB experiments (the droplet flame images for n-decane are similar to n-octane in terms of soot formation and flame structure and are not included in the present study). The needle-like glows on the sides of the flame in Fig. 7 are due to interactions between flames and supporting fibers. The ISS and GB images are reproduced at different scales, which are given at the bottom of the figure.

As shown in Fig. 7, the flame brightness increases with increasing D_o within the range 0.52 mm $\leq D_o \leq$ 0.85 mm (GB range), while the opposite trend is found for $D_o \geq$ 2.16 mm for the ISS images. This observation appears to indicate increasing soot formation with increasing D_o for the small droplets, while for the larger (ISS) droplets radiative losses keep the temperature down and limit sooting. For $D_o >$ 2.5 mm, a blue flame is visible soon after ignition, and the inner soot-enriched flame shows soot incandescence inside the blue flame. A radiative extinction-like effect (Nayagam et al. (2012)) is found for D_o = 3.61 mm shortly after ignition.

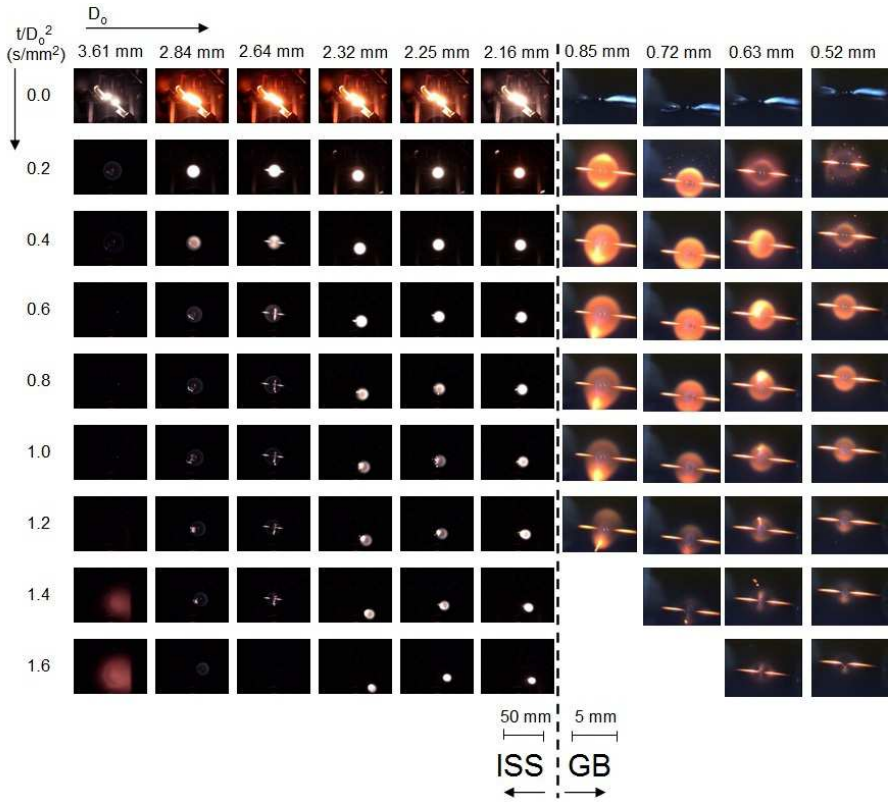

Figure 7. Selected color images of burning n-octane droplets with different initial droplet diameters.

Figure 8 displays the burning history recorded using back-lighting that clearly shows the sooting dynamics for n-octane droplets with various initial diameters. In the large droplet ISS experiments, soot shells are somewhat deformed as the hotwire igniter arms are retracted. This early deformation leads to later soot "tails" on the sides of the droplet. Also shown in Fig. 8 is a sequence from the ISS of a fiber-supported droplet (i.e., D_o = 2.64 mm). A noticeable external flow pattern is found after 0.4 s/mm^2. The effect of the fiber-induced flow is discussed below.

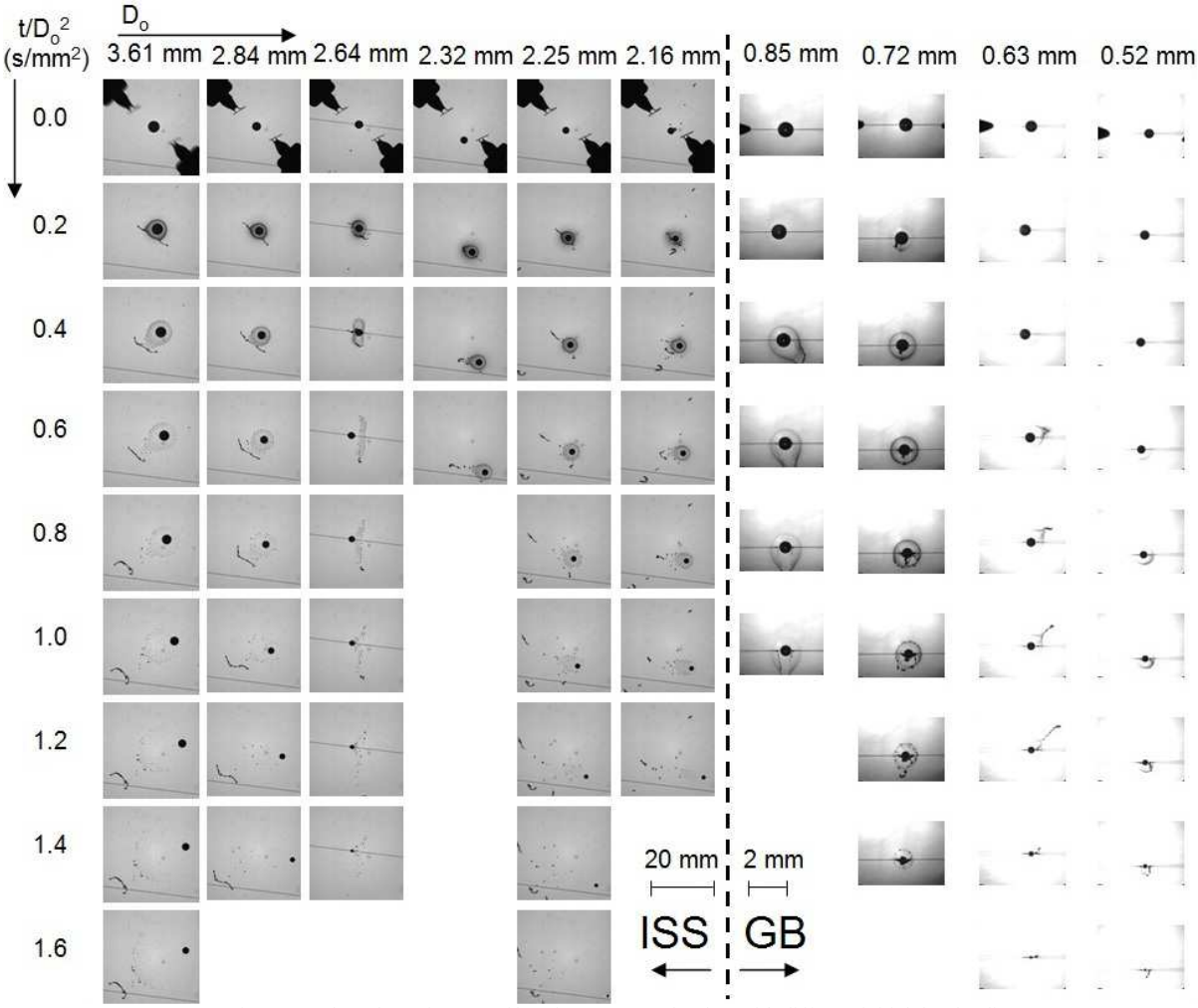

Figure 8. Selected BW images of burning n-octane droplets with different initial droplet diameters.

Figure 9a shows quantitative measurements of the evolutions of droplet diameter (or D^2) for n-octane with different initial diameters (0.52 mm ≤ D_o ≤ 3.61 mm) obtained from analyses of individual frames in the burning sequences (e.g., Fig. 8). It is evident from the trends that the droplet burning process is slowed as D_o increases. To more clearly show this influence of D_o on burning given that $K_o(t, D_o)$, the total burning time was divided into sections within which the evolutions of D^2 was linearized to obtain K_o for those sections. These time groups are identified in Figs. 9a and 10a (the latter for n-decane) by the dotted lines.

Figures 9b to 9e show burning rates averaged within the four time intervals in Fig. 9a. The burning rate clearly decreases with increasing D_o in each interval. As noted previously, two mechanisms are envisioned to bring about a variation of D_o on K_o. In the first, the fuel molecule residence time increases with D_o (Jackson et al. (1992)). In the absence of any other process that could influence heat transfer to the droplet (e.g., radiative losses), increasing soot formation would represent a lower heat release at the flame, less heat transfer to the droplet, and a lower burning rate. However, Fig. 7a shows comparatively less flame luminosity for D_o > 2 mm suggesting a *lower* sooting propensity as D_o further increases, yet Figs. 9b to 9e shows that K_o continues to decrease. While sooting may be decreasing for the larger droplets, concurrently the expansion of the flame makes radiative losses from it a potentially important mechanism to reduce heat transfer to the droplet. The fact that K_o does continue to decrease (cf, Fig. 9b to 9e) while the flame

luminosity also decreases indicates (Fig. 7) for $D_o > 2$ mm indicates that radiation may be responsible for the continued reduction of burning rate with increasing in this range of initial droplet diameter. The trends for n-decane shown in Fig. 10 are consistent with these trends.

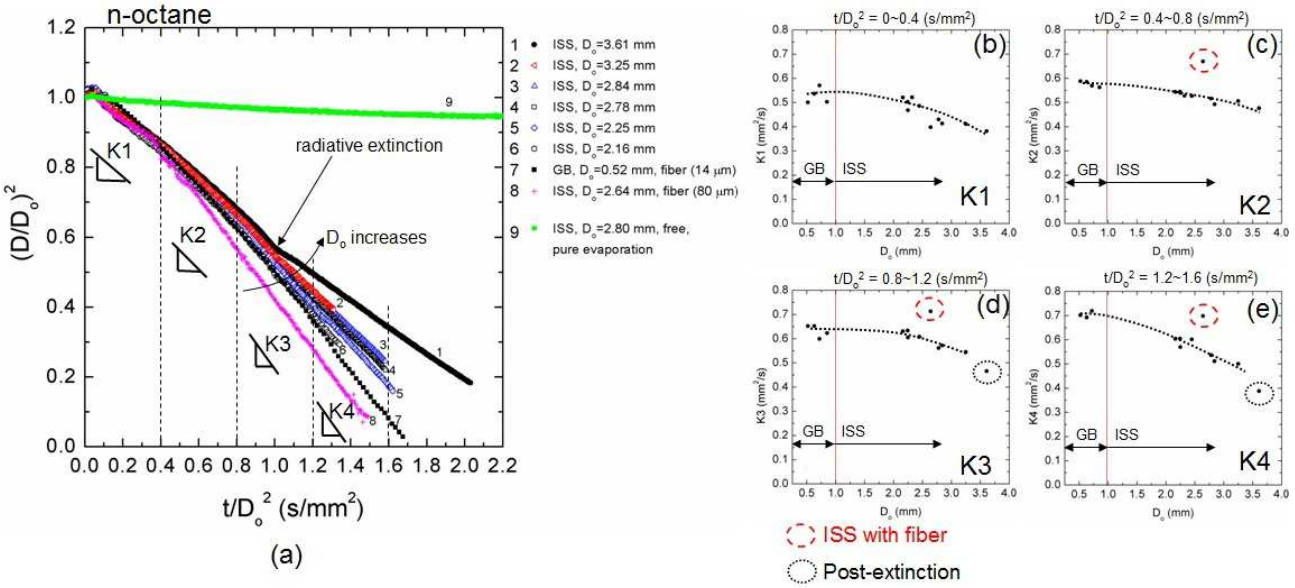

Figure 9. (a) Evolution of squared droplet sizes for spherically symmetric n-octane droplet flames with various initial droplet sizes; (b) to (e) are the local burning rates K1 to K4, respectively, obtained using linear fits in the regimes defined in graph (a).

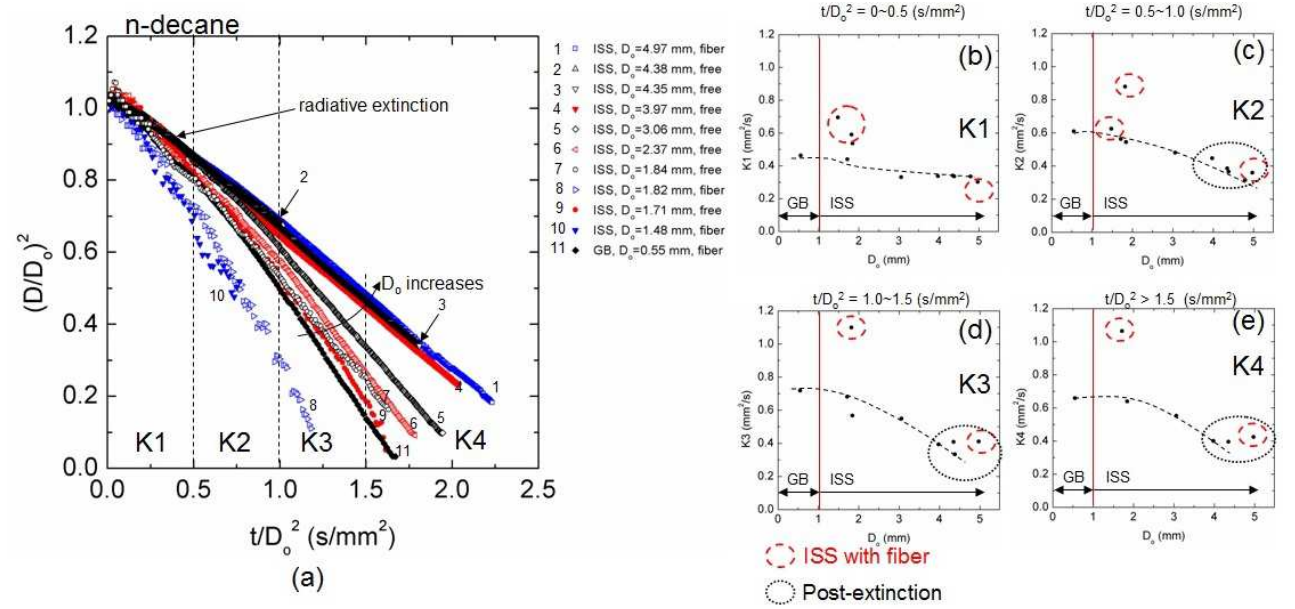

Figure 10. (a) Evolution of squared droplet sizes for spherically symmetric n-decane droplet flames with various initial droplet sizes; (b) to (e) are the local burning rates K1 to K4, respectively, obtained using linear fits in the regimes defined in graph (a).

With increasing heat loss from the flame for large droplets comes the prospect of extinction, which was found firstly by disappearance of the flame, and secondly by a noticeable decrease in the burning rate. Figures 9a, 9d and 9e show such a decrease for n-octane with $D_o = 3.61$ mm at about 1.0 s/mm^2. At larger times the octane burning rate is much lower, though the post-extinction burning rate is still higher than the rate of pure evaporation for n-octane as shown by the green data in Fig. 9a. For n-decane (Fig. 10a) when $D_o > 3.97$ mm the extinction process was more subtle yet still revealed by disappearance of the flame. The post-extinction burning rate for n-decane is about the same as for n-octane

(cf, Fig. 9d and 9e for n-octane and Figs. 10c, 10d and 10e for n-decane), though the pre-extinction burning rates are considerably lower for n-decane, most likely due in part to n-decane's higher liquid density. The extinction process for spherical droplet flames is an active area of current research (Nayagam et al. (2012); Farouk and Dryer (2012)).

Flame and soot standoff ratios (FSR = D_f/D, SSR = D_s/D) in Fig. 11 and 12 show the relative position of the flames and soot shells to the droplet surface. Figure 11a shows that the FSR of n-octane slightly decreases with increasing D_o. This trend may be caused by lower flame temperatures and thus smaller evaporation rates of larger droplets so that the flame boundary is situated closer to the droplet surface. Figure 11b shows the SSR for n-octane with different initial droplet diameters. The SSR increases with D_o over the D_o range investigated.

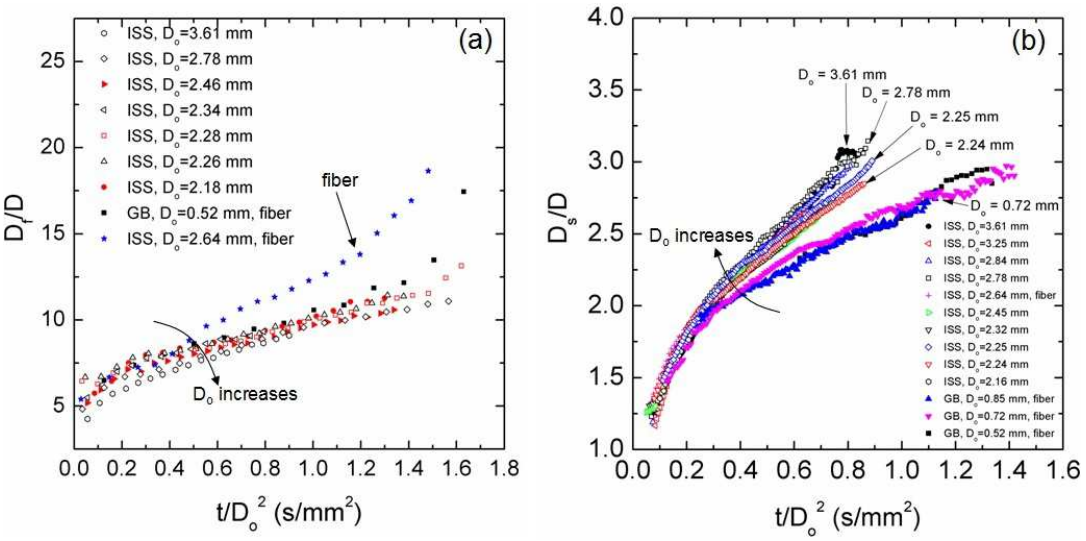

Figure 11. Effect of initial droplet diameter D_o on the flame standoff ratio (FSR = D_f/D) (a) and soot standoff ratio (SSR = D_s/D) (b) for spherically symmetric n-octane droplet flames.

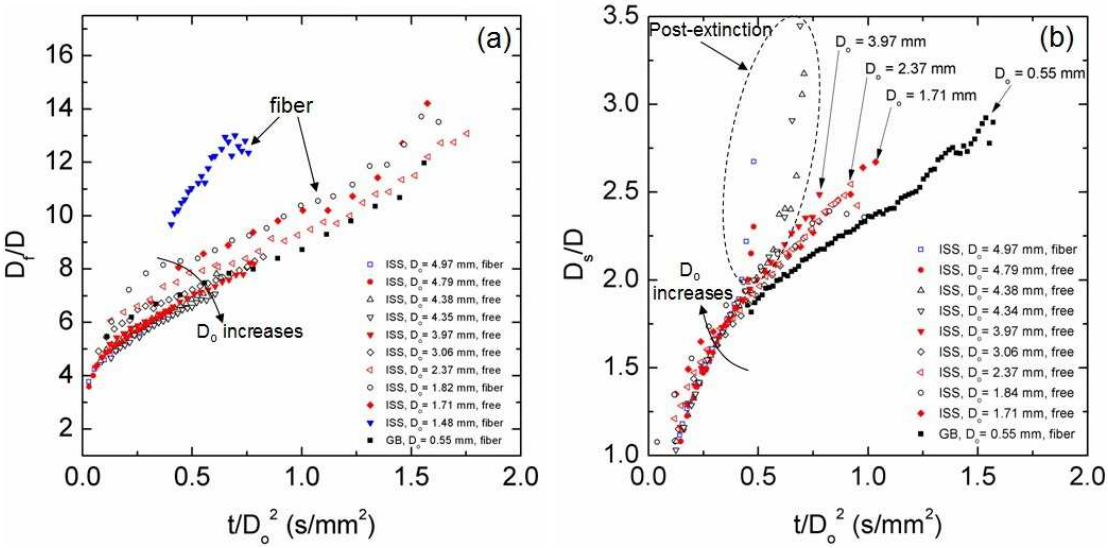

Figure 12. Effect of initial droplet diameter D_o on the flame standoff ratio (FSR = D_f/D) (a) and soot standoff ratio (SSR = D_s/D) (b) for spherically symmetric n-decane droplet flames.

The data in Fig. 11a and 12a (for n-octane and n-decane, respectively) suggest that the FSR, in general, decreases with increasing D_o. However, it is noticed for D_o = 1.71 and 2.37 mm in Fig. 12 that the FSR values are higher. These high FSR values are caused by the very bright flames of small droplets which saturate the flame boundaries such that it is very difficult to identify the actual "blue flame" boundary because of excessive image saturation. Figure 12b shows the SSR

for n-decane with various initial droplet diameters. Overall, the SSR slightly increases with D_o which is consistent with the observation for n-octane in Fig. 11b. The trends subsequent to extinction show the expansion of the soot shell though no further soot forms after radiative extinction. This radial expansion of the SSR after flame extinction may be evidence of diminished thermophoretic forces owing to disappearance of the hot flame (though the gases are still hot). The evaporation-induced force on soot aggregates would then balance thermophoresis at a larger relative distance from the droplet surface compared to if the flame existed.

Some of the ISS experiments were performed with droplets supported by 80 μm fibers as noted previously. This provided an opportunity to assess the influence of the support structure on the burning process. Regarding the evolution of D^2, Figs. 9a and 10a show several fiber-supported runs and Figs. 13a and 13b more clearly illustrate a comparison of free and fiber-supported droplets with the same approximate D_o value. The bigger is the droplet relative to the fiber the smaller will be an influence of the fiber on the burning rate. This general conjecture is consistent with the data in Figs. 13a and 13b, as well as Fig. 9 and 10 (cf, circled data in Figs. 10b-e and 11b-e). Flame diameters can also be affected by a support fiber as shown in Figs. 11a and 12a. In fact, for D_o ~5 mm (Fig. 13b), the burning rates for the free and fiber supported runs from the ISS are essentially identical. Regarding the FSR, larger FSRs for the fiber-supported data are likely due to a fiber-induced gas phase motion which results in slightly stronger fuel evaporation so that the flame is positioned farther away from the droplet surface. The insets to Figs. 13a and 13b (C and D) are photographs that illustrate the nature of this motion. As shown, the soot aggregates are markers for the flow and show a rather strong influence for smaller D_o (D_o ~2.6 mm for n-octane; D_o ~ 1.8 mm for n-decane). However, this effect appears to significantly decrease as the ratio of the droplet to the fiber diameter increases as shown by insets A and B in Fig. 13b.

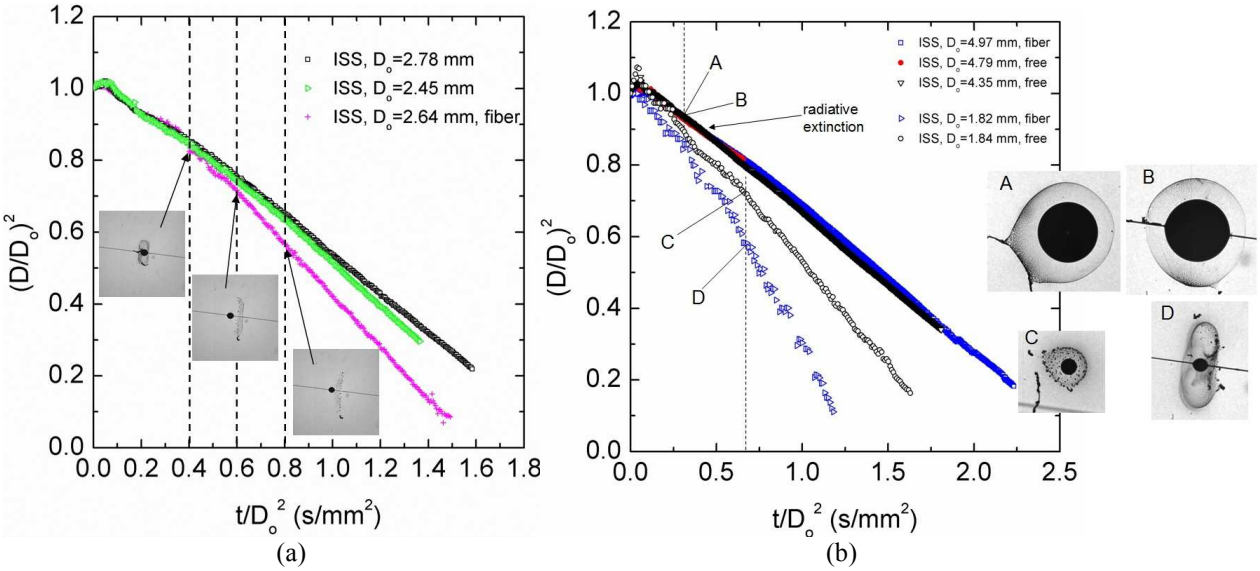

Figure 13. Effect of supporting fiber (SiC, 80 μm) on the droplet burning histories for (a) n-octane with D_o~ 2.6 mm, and (b) n-decane with D_o~ 4.97 mm (photo A with no fiber, B with a fiber) and D_o~ 1.8 mm (photo C with no fiber, D with a fiber).

The conventional interpretation of a fiber's influence on burning is from heat conduction through the fiber. A support fiber could also induce motion of the gas as noted above through its influence on transport of soot aggregates by the forces (e.g., thermophoresis) acting on the aggregates. This induced gas motion could potentially influence the droplet evaporation rate. The prospect for support fibers to induce gas motion and its influence on the burning process has not been previously considered, as prior work on fiber effects has focused primarily on conduction through the fiber.

4. Conclusions

The conclusions are the following.

1. Burning rates and FSRs decrease with increasing initial droplet diameters while SSRs increase with initial droplet diameters.

2. In the smaller droplet diameter range (0.52 mm $\leq D_o \leq$ 0.85 mm) where radiation effects are not significant, increasing initial droplet diameter leads to lower burning rate as D_o increases, most likely attributed to increased soot formation and a residence time effect.
3. In the larger droplet diameter range (2.16 mm $\leq D_o \leq$ 4.97 mm) where radiative losses become predominant the burning rate also decreases with increasing initial droplet diameter but the effect may be more linked to the increasing radiative losses and less heat transfer to the droplet than a direct role of sooting, which appears to be less for the large droplet diameter range.
4. The 80 μm SiC fiber used to tether the fuel droplet on the ISS can induce external convective flows around a small droplet (~ 1 to 2 mm) that significantly increases the burning rate and FSR. For a bigger droplet (D_o ~ 4.97 mm) the burning process is not strongly affected by the presence of the fiber.

Acknowledgements

This research was funded by the National Aeronautics and Space Administration under Grant No. NNX08AI51G. The authors thank Daniel Dietrich, Paul Ferkul, and Victoria Bryg of NASA and Wei-Chih Kuo and Anthony Savas of Cornell for their assistance during with the ISS experiments and image analyses.

References

Avedisian, C.T., Recent advances in soot formation from spherical droplet flames at atmospheric pressure, J. Propul. Power 16 (2000) 628-635.

Bae, J.H., Avedisian, C.T., Experimental study of the combustion dynamics of jet fuel droplets with additives in the absence of convection, Combust. Flame 137 (2004) 148-162.

Bae, J.H., Avedisian, C.T., Nonane droplet combustion with and without buoyant convection: Flame structure, burning rate and extinction in air and helium, Proc. Combust. Inst. 32 (2009) 2231-2238.

Dembia, C.L., Liu, Y.C., Avedisian, C.T., Automated data analysis for consecutive images from droplet combustion experiments, Image Anal. Stereol. 31 (2012) 137-148.

Farouk, T. and Dryer, F.L., "Cool flame" behavior for isolated alkane droplet combustion in microgravity, 28th Annual Meeting of the American Society for Gravitational and Space Research, New Orleans, LA, Nov. 28- Dec 2, 2012.

Godsave, G.A.E., Studies of the combustion drops in a fuel spray- the burning of single drops of fuel, Proc. Combust. Inst., 2, (1953) 818-830.

Hara, H., Kumagai, S., The effect of initial diameter on free droplet combustion with spherical flame, Proc. Combust. Inst., 25 (1994) 423–430.

Jackson, G.S., Avedisian, C.T., Yang, J.C., Observations of soot in droplet combustion at low gravity: heptane and heptane/monochloroalkane Mixtures, Int. J. Heat Mass. Trans., 35 (1992) 2017-2033.

Jackson G.S., Avedisian, C.T., The effect of initial diameter in spherically symmetric droplet combustion of sooting fuels, Proc. R. Soc. Lond. A 446 (1994) 255-276.

Kumagai, S., Sakai, T., Okajima, S., Combustion of free fuel droplets in a freely falling chamber, Proc. Combust. Inst., 13 (1971) 779-785.

Lee, K.-O., Manzello, S.L., Choi, M.Y., The effects of initial diameter on sooting and burning behavior of isolated droplets under microgravity conditions, Combust. Sci. Technol. 132 (1998) 139-156.

Liu, Y.C., Avedisian, C.T., A comparison of the spherical flame characteristics of sub-millimeter droplets of binary mixtures of n-heptane/iso-octane and n-heptane/toluene with a commercial unleaded gasoline, Combust. Flame 159 (2012) 770-783.

Liu, Y.C., Farouk, T., Savas, A.J., Dryer, F., Avedisian, C.T., On the spherically symmetrical combustion of methyl decanoate droplets and comparisons with detailed numerical modeling, Combust. Flame 160 (2013) 641-655.

Marchese, A.J., Dryer, F.L., Colantonio, R.O., Radiative Effects in Space-Based Methanol/Water Droplet Combustion Experiments, Proc. Combust. Inst., 27 (1998) 2627–2634.

Nayagam, V., Dietrich, D.L., Ferkul, P., Hicks, M.C., Williams, F.A., Can cool flames support quasi-steady alkane droplet burning? Combust. Flame 159 (2012) 3583-3588.

Turns, S.R., An Introduction to Combustion, 2nd ed., McGraw-Hill, New York, 2000, p. 376.